

INTERPRETABLE AUTOMATED DIAGNOSIS OF RETINAL DISEASE USING DEEP OCT ANALYSIS

PREPRINT, COMPILED JANUARY 14, 2022

Evan Wen^{1*} and Max Ehrlich²

¹The Pingry School

²Department of Computer Science, University of Maryland College Park

ABSTRACT

30 million Optical Coherence Tomography (OCT) imaging tests are issued every year to diagnose various retinal diseases, but accurate diagnosis of OCT scans requires trained ophthalmologists who are still prone to making errors. With better systems for diagnosis, many cases of vision loss caused by retinal disease could be entirely avoided. In this work, we develop a novel deep learning architecture for explainable, accurate classification of retinal disease which achieves state-of-the-art accuracy. Furthermore, we place an emphasis on producing both qualitative and quantitative explanations of the model's decisions. Our algorithm produces heatmaps indicating the exact regions in the OCT scan the model focused on when making its decision. In combination with an OCT segmentation model, this allows us to produce quantitative breakdowns of the specific retinal layers the model focused on for later review by an expert. Our work is the first to produce detailed quantitative explanations of the model's decisions in this way. Our combination of accuracy and interpretability can be clinically applied for better patient care.

1 INTRODUCTION

Every year there are approximately 30 million Optical Coherence Tomography (OCT) procedures done worldwide [1]. OCT is a non-invasive imaging test that yields cross-sectional slices of a patient's retina [2] which can be used to diagnose a multitude of retinal diseases. It is estimated that up to 11 million people in the United States have some form of macular degeneration [3]. The number of retinal disease patients continues to increase making the need for accurate diagnosis ever so more important. Accurate OCT diagnosis has traditionally been done by ophthalmologists trained to interpret these scans. However, the surplus of patients has been met with a shortage of ophthalmologists leading to occurrences of potentially unnecessary cases of vision loss [4].

Due to the shortage of experienced ophthalmologists and subjectivity in OCT classification, researchers have attempted to apply machine learning algorithms, most notably various types of Convolutional Neural Networks (CNN) [5]. Fauw et al. [6] used a 3D U-Net for segmentation combined with a 3D CNN to classify Normal, Choroidal Neovascularization (CNV), Macular Retinal Edema, Full Macular Hole, Partial Macular Hole, Central Serous Retinopathy(CSR), and Geographic Atrophy. Their models reached or exceeded the performance of human experts. Lu et al. [7] used ResNet-101 to classify Cystoid Macular Edema, Epiretinal Membrane, Macular Hole, and Serous Macular Detachment, their model outperformed two physicians. Nagasato et al. [8] used a deep convolutional neural network to detect a nonperfusion area in OCTA images. Li et al. [9] used ResNet50 to classify CNV, Diabetic Macular Edema (DME), Drusen, and Normal. Tsuji et al. [10] used a capsule network to classify CNV, DME, Drusen, and Normal. In addition, Wang et al. [11] used CliqueNet to classify Age-related Macular Edema (AMD), DME, and Normal. Yoo et al. [12] used Inception-V3 combined with CycleGAN for data augmentation to classify rarer retinal diseases.

A flaw common to these models is the lack of interpretability: they are black-boxes. To improve retinal disease patient care, machine learning models must be accurate but also more interpretable. A standalone diagnosis can leave patients skeptical of the model's validity. Another potential benefit of interpretability is when a model's interpretation is statistically suspicious, it can be flagged for review by a doctor for an extra level of validation, this requires **quantitative** as well as **qualitative** explanations. In this work, we present an accurate and interpretable deep learning model for classifying OCT scans. Using a combination of Gradient Weighted Class Activation Mapping (GradCAM) [13] and semantic segmentation we obtain detailed breakdowns of exactly which retinal layers the model used when making its decisions. This allows us to understand the specific behaviors the model learned and analyze why the model made incorrect decisions. Our method produces qualitative explanations, in the form of heatmaps with highlighted retinal layers, and quantitative explanations indicating the percent of model focus on each retinal layer. See Figure 1 for an overview of our algorithm. In summary, we contribute:

- A CNN architecture that achieves state-of-the-art results in OCT classification.
- A novel method for producing both **quantitative** and **qualitative** explanations of the machine generated diagnosis.

2 LITERATURE REVIEW

2.1 OCT Classification

Due to the shortage of experienced ophthalmologists and subjectivity in OCT classification, researchers have attempted to apply machine learning algorithms, most notably various types of Convolutional Neural Networks (CNN) [5]. Fauw et al. [6] used a 3D U-Net for segmentation combined with a 3D CNN

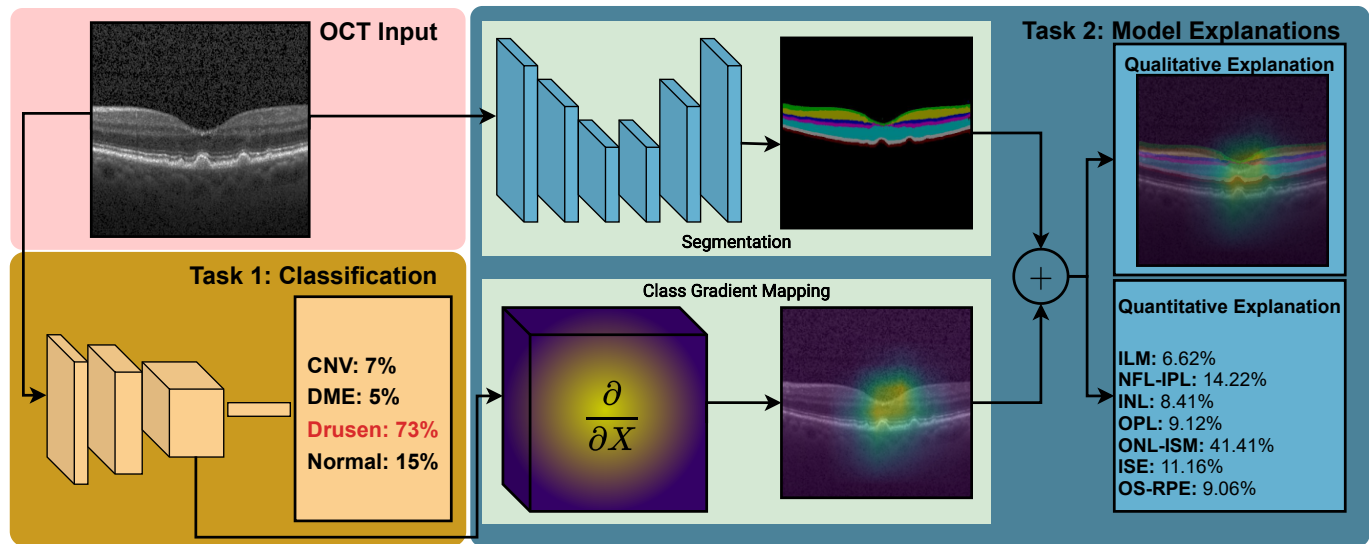


Figure 1: Our framework for generating accurate, interpretable OCT scan classifications.

to classify Normal, Choroidal Neovascularization (CNV), Macular Retinal Edema, Full Macular Hole, Partial Macular Hole, Central Serous Retinopathy (CSR), and Geographic Atrophy. Their models reached or exceeded the performance of human experts. Lu et al. [7] used ResNet-101 to classify Cystoid Macular Edema, Epiretinal Membrane, Macular Hole, and Serous Macular Detachment, their model outperformed two physicians. Nagasato et al. [8] used a deep convolutional neural network to detect a nonperfusion area in OCTA images. Li et al. [9] used ResNet50 to classify CNV, Diabetic Macular Edema (DME), Drusen, and Normal. Tsuji et al. [10] used a capsule network to classify CNV, DME, Drusen, and Normal. In addition, Wang et al. [11] used CliqueNet to classify Age-related Macular Edema (AMD), DME, and Normal. Yoo et al. [12] used Inception-V3 combined with CycleGAN for data augmentation to classify rarer retinal diseases. Our work contributes a new CNN architecture which achieves state-of-the-art performance for OCT classification. Furthermore, we achieve a new level of detail in producing model explanations. Previous works were limited to qualitative explanations in heatmaps. However, heatmaps have little to no use when one cannot understand the specific parts of the retina the model is looking at. Due to this constraint, we develop a segmentation-based algorithm for generating quantitative explanations.

2.2 CNN Visualization

Various approaches have been used to visualize the behaviours of CNNs. In Zeiler et al, a deconvolutional network was used to map network activations to the input pixel space and show the input patterns learned by the CNN [14]. Simonyan et al. visualized partial derivatives from predicted class scores and generated saliency maps [15]. Springenberg et al. used a deconvolution approach similar to Zeiler et al. for feature visualization of a CNN [16]. Zhou et al. introduced class activation mapping (CAM), a technique for generating localization maps using the global average pooled convolutional feature maps in the last convolutional

layer [17]. Selvaraju et al. generalized the CAM algorithm by making GradCAM, a technique that does not require a specific CNN architecture to develop explanations. CAM, however, requires a CNN with global average pooling followed by a single fully connected layer that outputs the prediction [13]. GradCAM first computes the gradient of the targeted output class with respect to the final convolutional layer’s feature map activations. Next, it performs pooling on the gradients to obtain neuron importance weights before performing a weighted combination of the feature maps to compute the GradCAM heatmap.

3 METHODOLOGY

Here we describe our algorithm to produce highly accurate, easily understandable diagnoses. Our algorithm depends on a classification model, GradCAM heatmaps, and a segmentation model which are now discussed in more detail.

3.1 Classification Model

For OCT image classification we build a CNN architecture based off an EfficientNetB2 backbone [18]. We choose the EfficientNet model because of its robust performance on the ImageNet-1k data set [19]. Since EfficientNet is designed for ImageNet classification, it outputs 1000 logits in the final layer. Therefore, we add two fully connected layers of sizes 100 and 4 with a softmax activation on the final layer to perform classification on four retinal diseases.

The full model is trained end-to-end with the Adam [20] Optimizer with a learning rate of 0.001 with the categorical cross-entropy loss function. We train the model for a total of 20 epochs. We use four methods for evaluating our models: accuracy, precision, recall, and F1 score.

Table 1: Results of our model measured in accuracy, precision, recall, and F1 score. A comparison with previous works is shown; the bold represents the highest scores for each metric.

Model	Accuracy	Precision	Recall	F1-Score
Ours	0.9979	0.9979	0.9979	0.9979
Kermany et. al Inception V3	0.961	0.96125	0.961	0.9625
Tsuji et. al Capsule Network	0.996	0.996	0.9961	0.9975
Li et. al ResNet-50	0.973	0.963	0.985	0.975

3.2 Gradient-Weighted Class Activation Mapping

A major focus of our work is to interpret predictions made by our classification models. We use Gradient-weighted Class Activation Mapping (GradCAM) [13] to produce heatmaps highlighting the regions the model utilized to make a prediction. The GradCAM algorithm utilizes the inputs to the model, the output of the final convolutional layer, and the output of the model prior to the softmax activation function. We overlay heatmaps on the original images to compare the model’s focus during classification of each disease. We also analyze why the model makes incorrect classifications by looking at its resulting heatmap.

3.3 Segmentation Model

To further interpret our model’s result, we employ a U-Net [21] architecture, pretrained for retinal layer segmentation [22]. Standalone GradCAM heatmaps give a general idea of where the model looked at, but by localizing the heatmap to specific retinal layers, we obtain both a clearer qualitative explanation of the model as well as a thorough quantitative explanation. The U-Net is trained to detect nine retinal layers: region above retina (RaR), inner limiting membrane (ILM), nerve fiber ending to inner plexiform layer (NFL-IPL), inner nuclear layer (INL), outer plexiform layer (OPL), outer nuclear layer to inner segment myeloid (ONL-ISM), inner segment ellipsoid (ISM), outer segment to retinal pigment epithelium (OS-RPE), and region below retina (RbR). The U-Net model is trained on DME scans from the data set presented in Srinivasan et al. [23] for 20 epochs.

3.4 Producing Explanations

We apply the segmentation model on our data set of OCTs before we overlay the GradCAM heatmaps on the segmentation maps. This allows us to obtain a visual breakdown of the model’s focus based on the retinal layers. We also calculate percentages of the model’s focus on each of the retinal regions excluding the regions above and below the retina. We choose to exclude these regions because they generally are less important for the model, but they have high enough area to potentially alter the percentages of the model’s focus. For each of the four retinal disease classifications, we obtain a mean model focus percentage for the seven retinal layers, denoted in Equation (1), during correct OCT classifications. F_i denotes the model’s focus on layer i . $S_{i,r,c}$ is a one-hot encoded integer as to whether the pixel at r, c is of retinal layer i , and $H_{r,c}$ is the value of the GradCAM heatmap at pixel r, c .

$$F_i = 100 * \frac{\sum_{r,c} S_{i,r,c} H_{r,c}}{\sum_{l=1}^7 \sum_{r,c} S_{l,r,c} H_{r,c}} \quad (1)$$

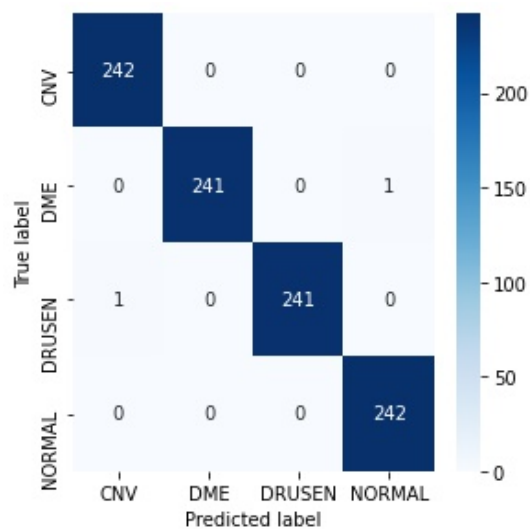


Figure 2: Confusion matrix from our classification model.

4 RESULTS AND DISCUSSION

4.1 Data Set

The OCT scans for this work come from the Kermany labeled OCT data set [24]. The data set contains four classes: Choroidal Neovascularization (CNV), Diabetic Macular Edema (DME), Drusen, and Normal (healthy). The data set utilizes Spectralis OCT machine scans from the Shiley Eye Institute of the University of California San Diego, the California Retinal Research Foundation, the Medical Center Ophthalmology Associates, the Shanghai First People’s Hospital, and the Beijing Tongren Eye Center. All images went through an extensive manual classification process by a cohort of retinal specialists to ensure correct labels.

We tested class-weighting due to the imbalance in the data set. Drusen had significantly less scans in the training set whereas CNV had significantly more scans. The class weights were evaluated based on the number of scans in the training set. We took the highest number of scans for any label which was 37,205 for CNV and divided by the number of scans for each of the labels to obtain the class weights of 1, 3.279, 4.318, and 1.414 for CNV, DME, Drusen, and Normal respectively.

4.2 Data Preprocessing

The Kermany data set contains a total of 84,484 OCT scans. The data was split into 968 test images and 83,484 training images. Of the 83,484 training images, 37,205 were labeled as CNV, 11,348 were DME, 8616 were Drusen, and 26,315 were Normal.

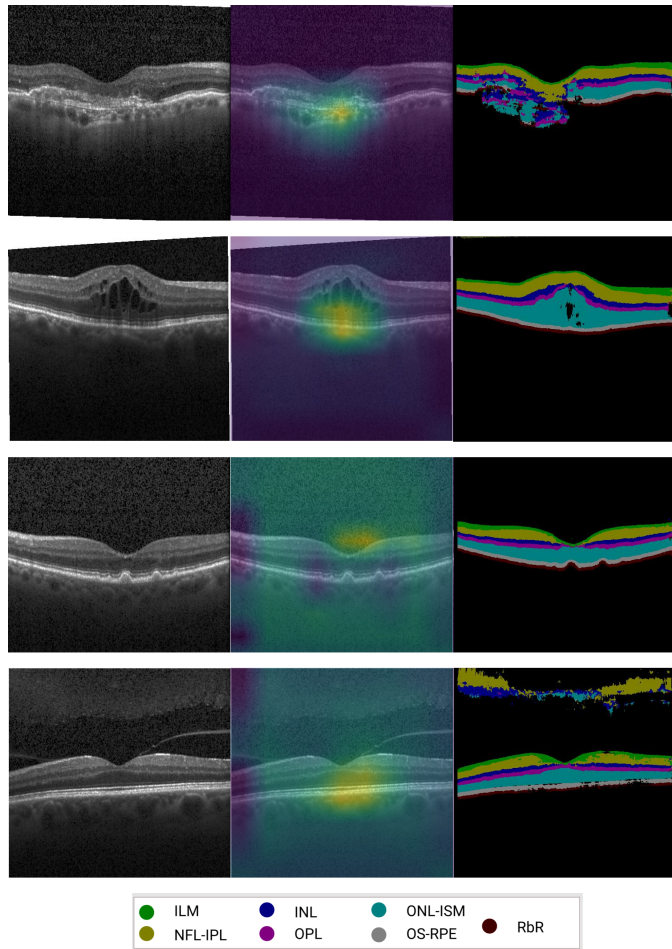


Figure 3: Heatmaps and segmentation maps from the OCT scans. Left: OCT scan, Middle: GradCam heatmap, Right: segmentation map. The scans are CNV, DME, Drusen, and Normal from top to bottom.

The test data consists of 242 images of each class. Scans are separated by their correct labels into folders containing JPEG image files. The dimensions of the original images varied from 384-1536 pixels wide and 496-512 pixels high. All images are rescaled to 260 pixels wide and 260 pixels high using bilinear interpolation. The training data is processed in batches of size 64.

4.3 Results of the Classification Models

Table 1 shows the state-of-the-art performance of our classification model. The per-class performance of the model is shown in Figure 2. As seen in Figure 2, the model makes only two errors: one mistaking Drusen for CNV and one mistaking DME for Normal. The model performs more accurately than the models presented by Kermany et al. [24], Tsuji et al. [10], and Li et al [9] who were trained to classify the same four diseases.

4.4 Qualitative Interpretability Results

Figure 3 shows GradCAM heatmaps and segmented OCT scans of each classification. Heatmaps from the Drusen and Normal

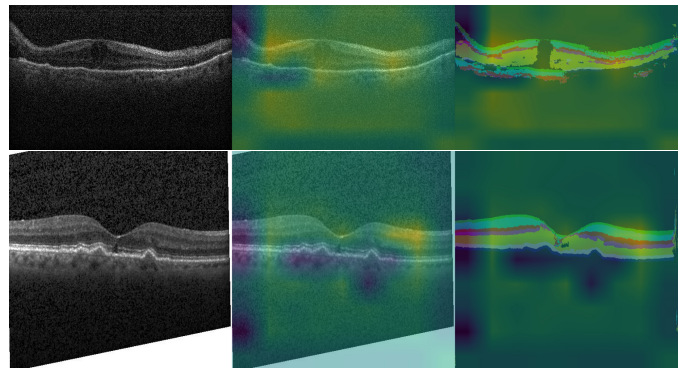


Figure 4: The two misclassifications from our model. Left: OCT scan. Middle: OCT scan with heatmap overlaid, Right: Segmentation map with heatmap overlaid. The first row is a DME scan which the model predicted Normal. The second row is a Drusen scan which the model predicted CNV.

scans have less centralized focus, but they still place an emphasis on the center of the scan. In the CNV classification, the model has the highest focus on the bottom-most layer of the retina. In the DME classification, the model still focuses on the bottom layer but also focuses on the intraretinal fluid. In the Drusen classification, the model does not have as much central focus. In the Normal classification, the model has more central focus than the Drusen classification. The model looks at the center of the scan to make the Normal classification.

The U-Net model performs well with segmentation on DME, Drusen, and Normal. The model is able to accurately detect each of the retinal layers. The model, however, does have some confusion on the region above the retina on the Normal scan. The scan appears to have some noise in the upper region which is captured in the segmented scan. The CNV scan is the least accurate of the segmented scans. The model has significant difficulty detecting the retinal layers in the irregular subretinal region. The model’s difficulty with the CNV and Normal scans are likely due to the U-Net being unfamiliar with these type of scans. Given that the U-Net was trained only on DME scans, it makes sense that the U-Net does not perform as well on CNV and Normal scans. We explain how the inaccuracies in segmentation affect the interpretability algorithm in the next section.

4.5 Quantitative Interpretability Results

Next, we apply our full algorithm to produce quantitative explanations. Table 2 shows the F_i (Equation (1)) values for correct classifications of each type. In all classifications, the ONL-ISM layer is the most focused followed by the NFL-IPL layer. This is likely due to these two regions occupying the most space in the scans. The rest of the layers have some variance between the diseases. CNV has the highest F_i values for INL, OPL, and OS-RPE. DME has the highest F_i for ONL-ISM. Drusen has the highest F_i for ILM and NFL-IPL. Normal has the highest F_i for ISE. In a sense, the interpretability of the model is similar to the reasoning of a human ophthalmologist. A human ophthalmologist looks at certain regions in the scan to make a decision, some regions more important than others. Our model, unlike previous

Table 2: The model’s mean focus on each of the retinal layers when making correct classifications. Each column provides a breakdown of the model’s focus for correct classifications of each disease.

Layer	CNV	DME	Drusen	Normal
ILM	5.39%	6.62%	10.87%	7.96%
NFL-IPL	14.03%	14.22%	23.67%	20.48%
INL	12.26%	8.41%	10.00%	8.75%
OPL	12.73%	9.12%	10.70%	9.97%
ONL-ISM	35.90%	41.41%	27.74%	30.91%
ISE	9.90%	11.16%	9.61%	13.18%
OS-RPE	9.78%	9.06%	7.42%	8.75%

Table 3: The model’s focus during its two misclassifications. The first misclassification is the model predicting Normal on a DME scan. The first deviation column represents how many standard deviations the values in the first column are from the mean when correctly classifying Normal scans. The second misclassification is the model predicting CNV instead of Drusen. The second deviation column represents how many standard deviations the values in the third column are from the mean when correctly classifying CNV scans.

Layer	Misclass. 1	Deviation	Misclass. 2	Deviation
ILM	16.76%	5.82	9.95%	1.74
NFL-IPL	18.67%	-0.60	21.43%	1.66
INL	14.54%	3.01	11.96%	-0.07
OPL	7.94%	-1.66	12.20%	-0.14
ONL-ISM	33.52%	0.85	28.00%	-1.14
ISE	3.76%	-5.20	9.05%	-0.31
OS-RPE	4.80%	-3.07	7.41%	-0.79

ones, can give the same level of explanation, highlighting which regions are important for the classification.

Now we demonstrate that our model is learning the correct areas of the scan to focus on. CNV involves the growth of new blood vessels from the choroid that result in breaking the Bruch membrane and the subretinal space. This is consistent with our model which says that CNV has the highest focus of all diseases on the OS-RPE, the lowest region of the retina. DME occurs with excess fluid build up in the macula of the eye, located at the center of the retina. Again, this is consistent with our model which says that DME has the highest focus of all diseases on the ONL-ISM, the layer in the middle of the retina. Drusen occurs with deposits of waste present which cause elevated RPE. While Drusen has low focus for the ISE and OS-RPE, it has the highest focus on the two regions at the top. This is likely because the model analyzes the peaks of the elevated RPE "humps" which occur closely to the top of the OCT scan. Finally, it makes sense that Normal does not have the most focus on many regions. This is because the model must first rule out the three diseases before making a Normal classification, similar to a human ophthalmologist.

Figure 4 and Table 3 explain the model’s incorrect classifications. The GradCAM overlaid heatmaps show the model has no specific area of focus in both classifications. The model’s focus is nearly evenly distributed across the entire OCT scan instead of a centralized area commonly seen during correct classifications.

The deviations from the second column of Table 3 show the ILM, INL, ISE, and OS-RPE are significantly off from the mean F_i for correct Normal classifications. The large deviations show that the model’s explanation is too different from the explanation of a correct classification. When a prediction has a statistically suspicious explanation, the scan should be flagged for further review; the model’s prediction should not be trusted. On the other hand, the other set of deviations from the DME scan mistaken CNV appear to be much closer. This is due to the correct CNV classifications generally having higher variance in their F_i . As can be seen in Figure 3, the segmented CNV scan are the least accurate. The lack of accuracy in CNV scan segmentation leads to the high variability in F_i scores. While the model appears to have a statistically sound quantitative explanation for this classification, the qualitative explanation in the heatmap shows the model is not confident when making this prediction.

5 CONCLUSION

In this work, we presented a very accurate model for classifying OCT scans of CNV, DME, Drusen, and Normal. We utilized GradCAM and a U-Net semantic segmentation network to reach a new level of interpretability. Our model performs at an accuracy of 99.79%, higher than all previous works. Our GradCAM heatmaps generate qualitative explanations by demonstrating the important areas of the OCT scans our model utilized. After we combined the heatmaps with the segmented OCT scans, we discovered the patterns learned by the model when making correct scans through the mean focus metric. We calculated the average model focus on each of the detected retinal layers when making correct classifications. Analyzing the average model focus shows the model operates very similar to a human ophthalmologist. When comparing the model’s focus on incorrect classifications to the model’s focus on correct classifications, we sometimes noticed potential reasoning as to why the model misclassified a scan. This new level of interpretability in our model brings deep learning one step closer to real clinical application; patients and doctors can be more confident that they are getting a correct diagnosis. In addition to an accurate diagnosis, patients deserve qualitative and quantitative information as to why the model made such diagnosis rather than a standalone diagnosis. Even if a patient is given a heatmap, they still might not know where the anomalies are. We also show that our explanations can be used to predict whether the model’s classification is correct. Future work would involve training and evaluating a similar classification model on a more diverse data set. As mentioned in the introduction, deep learning has significant potential in diagnosing more retinal conditions. For better quantitative results, the accuracy of the segmentation model could be improved. The U-Net segmentation model we used was inaccurate on CNV and Normal scans, resulting in sometimes unclear quantitative explanations. Future work could train the model on a data set with more diseases or utilize newer segmentation algorithms such as the segmentation transformer presented by Zheng et al [25]. Another possible experiment would be to place eye trackers on human ophthalmologists to generate heatmaps from humans and compare with our model.

REFERENCES

- [1] J. Fujimoto and E. Swanson. The Development, Commercialization, and Impact of Optical Coherence Tomography. *Invest Ophthalmol Vis Sci*, 57(9):OCT1–OCT13, 07 2016.
- [2] J. G. Fujimoto, C. Pitris, S. A. Boppart, and M. E. Brezinski. Optical coherence tomography: an emerging technology for biomedical imaging and optical biopsy. *Neoplasia*, 2(1-2):9–25, 2000.
- [3] Age-related macular degeneration: Facts & figures, Jan 2020. URL <https://www.brightfocus.org/macular/article/age-related-macular-facts-figures>.
- [4] B. Foot and C. MacEwen. Surveillance of sight loss due to delay in ophthalmic treatment or review: frequency, cause and outcome. *Eye (Lond)*, 31(5):771–775, May 2017.
- [5] Alex Krizhevsky, Ilya Sutskever, and Geoffrey E. Hinton. Imagenet classification with deep convolutional neural networks. In F. Pereira, C. J. C. Burges, L. Bottou, and K. Q. Weinberger, editors, *Advances in Neural Information Processing Systems 25*, pages 1097–1105. Curran Associates, Inc., 2012.
- [6] Jeffrey De Fauw et al. Clinically applicable deep learning for diagnosis and referral in retinal disease, Aug 2018. URL <https://www.nature.com/articles/s41591-018-0107-6/>.
- [7] Wei Lu, Yan Tong, Yue Yu, Yiqiao Xing, Changzheng Chen, and Yin Shen. Deep Learning-Based Automated Classification of Multi-Categorical Abnormalities From Optical Coherence Tomography Images. *Translational Vision Science & Technology*, 7(6):41–41, 12 2018. ISSN 2164-2591. doi: 10.1167/tvst.7.6.41. URL <https://doi.org/10.1167/tvst.7.6.41>.
- [8] D. Nagasato et al. Automated detection of a nonperfusion area caused by retinal vein occlusion in optical coherence tomography angiography images using deep learning. *PLoS One*, 14(11):e0223965, 2019.
- [9] F. Li et al. Deep learning-based automated detection of retinal diseases using optical coherence tomography images. *Biomed Opt Express*, 10(12):6204–6226, Dec 2019.
- [10] T. Tsuji et al. Classification of optical coherence tomography images using a capsule network. *BMC Ophthalmol*, 20(1):114, Mar 2020.
- [11] Depeng Wang and Liejun Wang. On oct image classification via deep learning. *IEEE Photonics Journal*, 11(5): 1–14, 2019. doi: 10.1109/JPHOT.2019.2934484.
- [12] T. K. Yoo, J. Y. Choi, and H. K. Kim. Feasibility study to improve deep learning in OCT diagnosis of rare retinal diseases with few-shot classification. *Med Biol Eng Comput*, 59(2):401–415, Feb 2021.
- [13] Ramprasaath R. Selvaraju, Abhishek Das, Ramakrishna Vedantam, Michael Cogswell, Devi Parikh, and Dhruv Batra. Grad-cam: Why did you say that? visual explanations from deep networks via gradient-based localization. *CoRR*, abs/1610.02391, 2016. URL <http://arxiv.org/abs/1610.02391>.
- [14] Matthew D. Zeiler and Rob Fergus. Visualizing and understanding convolutional networks. *CoRR*, abs/1311.2901, 2013. URL <http://arxiv.org/abs/1311.2901>.
- [15] Karen Simonyan, Andrea Vedaldi, and Andrew Zisserman. Deep inside convolutional networks: Visualising image classification models and saliency maps, Apr 2014. URL <https://arxiv.org/abs/1312.6034>.
- [16] Jost Tobias Springenberg, Alexey Dosovitskiy, Thomas Brox, and Martin Riedmiller. Striving for simplicity: The all convolutional net, 2014.
- [17] B. Zhou, A. Khosla, Lapedriza. A., A. Oliva, and A. Torralba. Learning Deep Features for Discriminative Localization. *CVPR*, 2016.
- [18] Mingxing Tan and Quoc V. Le. Efficientnet: Rethinking model scaling for convolutional neural networks. *CoRR*, abs/1905.11946, 2019. URL <http://arxiv.org/abs/1905.11946>.
- [19] Jia Deng, Wei Dong, Richard Socher, Li-Jia Li, Kai Li, and Li Fei-Fei. Imagenet: A large-scale hierarchical image database. In *2009 IEEE conference on computer vision and pattern recognition*, pages 248–255. Ieee, 2009.
- [20] Diederik P. Kingma and Jimmy Ba. Adam: A method for stochastic optimization. *CoRR*, abs/1412.6980, 2015.
- [21] Olaf Ronneberger, Philipp Fischer, and Thomas Brox. U-net: Convolutional networks for biomedical image segmentation. *CoRR*, abs/1505.04597, 2015. URL <http://arxiv.org/abs/1505.04597>.
- [22] Abhijit Guha Roy et al. Relaynet: Retinal layer and fluid segmentation of macular optical coherence tomography using fully convolutional network. *CoRR*, abs/1704.02161, 2017. URL <http://arxiv.org/abs/1704.02161>.
- [23] Pratul P. Srinivasan et al. Fully automated detection of diabetic macular edema and dry age-related macular degeneration from optical coherence tomography images. *Biomed. Opt. Express*, 5(10):3568–3577, Oct 2014. doi: 10.1364/BOE.5.003568. URL <http://www.osapublishing.org/boe/abstract.cfm?URI=boe-5-10-3568>.
- [24] Daniel S Kermany et al. Identifying medical diagnoses and treatable diseases by image-based deep learning. *Cell*, 172(5):1122–1131, 2018.
- [25] Sixiao Zheng et al. Rethinking semantic segmentation from a sequence-to-sequence perspective with transformers. *CoRR*, abs/2012.15840, 2020. URL <https://arxiv.org/abs/2012.15840>.